

# Privacy-Net: An Adversarial Approach For Identity-obfuscated Segmentation

<sup>1</sup>Bach Ngoc Kim, <sup>1</sup>Jose Dolz, <sup>2</sup>Pierre-Marc Jodoin and <sup>1</sup>Christian Desrosiers

<sup>1</sup>LIVIA Lab, École de Technologie Supérieure (ETS)

<sup>2</sup>VITAL Lab, Université de Sherbrooke

ngoc-bach.kim.1@ens.etsmtl.ca  
jose.dolz@etsmtl.ca  
pierre-marc.jodoin@usherbrooke.ca  
christian.desrosiers@etsmtl.ca

## Abstract

This paper presents a privacy-preserving network oriented towards medical image analysis. Our approach is based on adversarial learning which encodes images to obfuscate the patient identity while preserving enough information for a target task. Our novel architecture is composed of three components: 1) an encoder network which removes identity-specific features from input medical images, 2) a discriminator network that attempts to identify the subject from the encoded images, 3) a medical image analysis network which analyzes the content of the encoded images (segmentation in our case). By simultaneously fooling the discriminator and optimizing the medical analysis network, the encoder learns to remove privacy-specific features while keeping those essentials for the target task. Our approach is illustrated on the problem of segmenting brain MRI from the large-scale Parkinson Progression Marker Initiative (PPMI) dataset. Using longitudinal data from PPMI, we show that the discriminator learns to heavily distort input images while allowing for highly accurate segmentation results.

## 1 Introduction

Machine learning models like deep convolutional neural networks (CNNs) have achieved outstanding performances in complex medical imaging tasks such as segmentation, registration, and disease detection (Zhou, Greenspan, and Shen 2017; Litjens et al. 2017). However, privacy restrictions on medical data including images impede the development of centralized cloud-based image analysis systems, a solution that has its share of benefits: no on-site specialized hardware, immediate trouble shooting or easy software and hardware updates, among others.

While server-to-client encryption can prevent attacks from outside the system, it cannot prevent cybercriminals within the system from gaining access to private medical data. Nowadays, the standard approach to obfuscate the identity of a patient is to anonymize its data. In case of images, this is done by removing the patient-related DICOM tags or by converting it into a tag-free format such as PNG or NIFTI. However, as shown by Kumar et al. (Kumar et al. 2018) and further illustrated in this paper, the raw content of an image can be easily used to recover the identity of a person with up to 97% of accuracy.

A recent solution to such problem has been federated learning (McMahan et al. 2017), which allows to collaboratively train a centralized model while keeping the training data decentralized. The idea behind this strategy is to transfer the training gradients of a data instead of the data itself. While such approach is appealing to train a neural network with data hosted in different hospitals, it does not allow the use of a centralized cloud-based model for making prediction at test time.

In this paper, we propose a system that encodes medical images into a format that preserves the identity of a patient while keeping enough semantic information to analyze its content with high accuracy. We achieve this with an adversarial learning approach inspired by generative adversarial networks (GAN) (Luc et al. 2016; Goodfellow et al. 2014; Ganin et al. 2016) but with two main differences. As illustrated in Fig. 1, instead of being a two-player game, our system involves three players: i) an image encoder, ii) a discriminator and iii) a medical image analysis network (a segmentation CNN in our case). Whereas the encoder’s objective is to obfuscate the content of a raw input image, the goal of the discriminator is to determine whether two images come from the same patient or not. The third player is a network which analyzes the content of the encoded image. As such, while the encoder tries to fool the discriminator, it must preserve enough information to allow the third network to successfully analyze its content. At test time, the encoder network is deployed on the client side which converts a raw image  $x$  into an encoded (and yet secure) image  $z$ . Thereafter,  $z$  is transferred to the cloud-based server where the segmentation network is deployed. The resulting segmentation map  $\hat{y}$  is then sent back to the client.

The major contributions of this work are as follows:

- We present the first privacy-preserving model for semantic image segmentation. Obfuscating identity while preserving task-specific information is particularly challenging for segmentation, which requires to assign a label for each image pixel.
- Our model proposes a novel architecture combining two CNNs for the encoder and segmentation networks with a Siamese CNN for the discriminator. This Siamese discriminator learns identity-discriminative features from

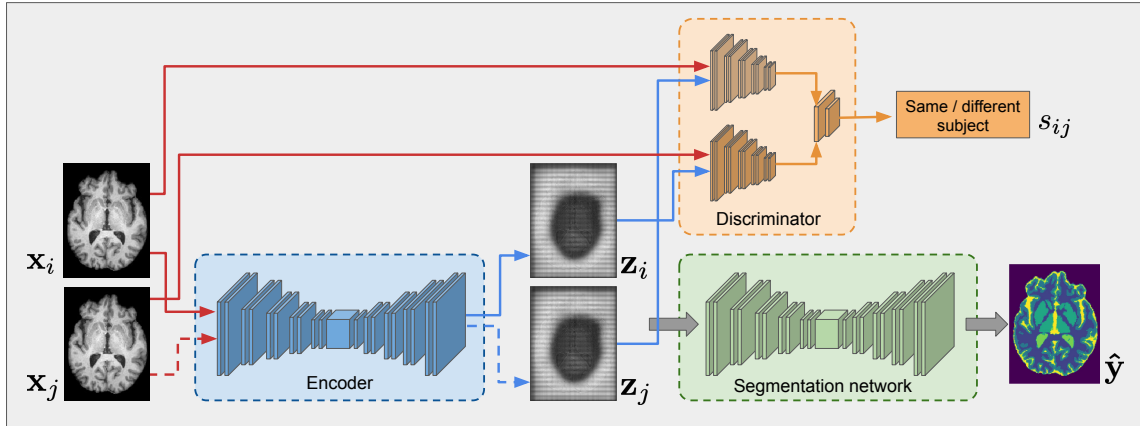


Figure 1: Training configuration of our proposed system: a) an encoder network  $E$  converts input images  $\mathbf{x}_i$  and  $\mathbf{x}_j$  into two new images  $\mathbf{z}_i$  and  $\mathbf{z}_j$ , b) the discriminator network  $D$  tries to determine if the input images it is fed with come from the same patient ( $s_{ij} = 1$ ) or not ( $s_{ij} = 0$ ) and c) the segmentation network  $S$  segments the encoder images. At test time (dotted lines), the discriminator is removed from the system and the encoder and the segmentation network are fed with a single image.

images pairs instead of a single image, allowing us to have a variable number of classes (i.e., subject IDs). Unlike the work in (Oleszkiewicz et al. 2018), our model is trained using both an adversarial Siamese loss and a task-specific loss, thereby providing encoded images that obfuscate identity while preserving the information required for the target task.

- We demonstrate that the privacy-preserving encoder learned with a given dataset can be used to encode images from another dataset, and that these encoded images are useful to update the segmentation network.

The next section gives an overview of related works on privacy-preserving models for image-related tasks, with a particular emphasis on adversarial learning techniques. Section 3 then presents the proposed model and loss functions used for training. In Section 4, we demonstrate the usefulness of our model on the problem of brain MRI segmentation from two benchmark datasets. Last, we conclude with a summary and discussion of key results.

## 2 Related Work

**Privacy preserving in visual tasks.** Traditional methods to preserve privacy rely on cryptographic approaches (Ziad et al. 2016; Wang et al. 2017) which create local homomorphic encryptions of visual data. Although these methods perform well in some applications, homomorphic cryptosystems typically incur high computational costs (Paillier 1999) and are mostly restricted to simple linear classifiers. This limits their usability in scenarios requiring more complex models like deep neural networks. Another solution consists in extracting feature descriptors from raw images, which are then transferred to the encrypted dataset server (Hsu, Lu, and Pei 2011). Nevertheless, sensitive information from original images can be still recovered from standard features, making these systems vulnerable to cyberattacks. An alternative strategy is to employ low-resolution images (Dai et al. 2015; Chen et al. 2016) or image filtering techniques (Butler et al. 2015; Jalal, Uddin, and Kim 2012) to degrade sensitive

information. However, since these approaches also reduce the quality of the visual content, they are limited to a reduced set of tasks such as action or face expression recognition. More recently, McClure et al. (McClure et al. 2018) proposed using continual learning to circumvent the issue of privacy preservation in the context of multi-center brain tumor segmentation. Nevertheless, unlike our method, their approach is not directly optimized to obfuscate identity from visual data.

**Federated learning** Federate learning has recently emerged as a solution to build machine learning models based on distributed data sets while preventing data leakage (Xie et al. 2014; Konecný et al. 2016; Hesamifard, Takabi, and Ghasemi 2017; McMahan et al. 2016; Vepakomma et al. 2018; Yang et al. 2019). With this approach, the learning process involves collaboration from all the data owners without exposing their data to others. This can typically be achieved by sharing the architecture and parameters between the client and server during training, along with intermediate representations of the model that may include the gradients, activations and weight updates. Thus, the client downloads the model from the server and updates the weights based on its local data. Yet, a major drawback of these strategies is their huge requirements for network bandwidth, memory and computational power, which strongly limits their scalability.

**Privacy preserving with adversarial learning.** The recent success of adversarial learning has led to the increased adoption of this technique for the protection of sensitive information, particularly in visual data. Xu et al. (Xu et al. 2019) proposed to add carefully-designed noise to gradients during the learning procedure to train a differentially-private GAN in the context of image recognition. An unsupervised utility loss is employed for training in (Raval, Machanavajjhala, and Cox 2017), based on the assumption that removing private characteristics from an image while

minimizing changes to the rest of the image yields encoded representations that can be used to learn a target task. However, since the encoding is performed independently of the task, it is potentially sub-optimal for this task. Other works (Pittaluga, Koppal, and Chakrabarti 2019; Wu et al. 2018; Yang et al. 2018; Roy and Boddeti 2019) have leveraged adversarial training to jointly optimize privacy and utility objectives. In these works, the mapping functions for the adversarial and task-specific terms are standard classification models where the number of classes is fixed. In (Chen, Konrad, and Ishwar 2018), a model which integrates a Variational Autoencoder (VAE) and a GAN is proposed to create an identity-invariant representation of face images. To explicitly control the features to be preserved, they include a discriminator which must predict the identity of the subject in a generated image. As the number of possible labels corresponds to the number of subjects to identify, this approach is not suitable for large-scale applications as the one considered in our work. To alleviate this problem, (Oleszkiewicz et al. 2018) instead uses a Siamese architecture for the discriminator, which predicts whether two encoded images come from the same subject. In this previous work, an auto-encoder loss is employed as task-agnostic utility objective to avoid the encoder from generating trivial images. In contrast, our privacy-preserving method considers a loss specific to the task of semantic segmentation.

### 3 Methodology

#### Proposed system

As shown in Fig. 1, our system implements a three-player zero-sum game where each player is an independent CNN. At the input of our system is a raw image  $\mathbf{x} \in \mathbb{R}^{H \times W \times D}$  (in our case a 3D T1 MR image). During training, images come in pair  $(\mathbf{x}_i, \mathbf{x}_j) \in \mathcal{X}^2$ ,  $i \neq j$ , and are associated to a binary target  $s_{ij}$  which is 1 when  $\mathbf{x}_i$  and  $\mathbf{x}_j$  come from the same patient and 0 otherwise. Each image is also associated with a ground-truth segmentation map pair  $(\mathbf{y}_i, \mathbf{y}_j)$ . As mentioned in Section 4, pairs of images from the same patient are not identical as they were acquired during different acquisition sessions, often months apart.

The first player is an encoder network  $E$  parameterized by  $\theta_E$ . The output of the encoder is an encoded image  $\mathbf{z} \in \mathbb{R}^{H \times W \times D}$ . While training the system, the encoder is fed with a pair of images  $(\mathbf{x}_i, \mathbf{x}_j)$  and returns two encoded images  $\mathbf{z}_i$  and  $\mathbf{z}_j$ . Here,  $\mathbf{x}_i$  and  $\mathbf{x}_j$  are processed individually and not concatenated together.

The second player is the Siamese discriminator network  $D$  with parameters  $\theta_D$ , which is fed with a pair of images. The goal of this network is to determine if the two images come from the same patient or not. By fooling  $D$  (i.e., maximizing its loss), the encoder provides transformed images that cannot be used to identify patient. Let  $\mathbf{z} = E(\mathbf{x})$ , to learn all possible cases,  $D$  is given six different types of image pairs, namely:  $(\mathbf{x}_i, \mathbf{x}_j)$ ,  $(\mathbf{z}_i, \mathbf{z}_j)$ ,  $(\mathbf{x}_i, \mathbf{z}_i)$ ,  $(\mathbf{x}_j, \mathbf{z}_j)$ ,  $(\mathbf{x}_i, \mathbf{z}_j)$  and  $(\mathbf{x}_j, \mathbf{z}_i)$ .

Last, the third player is the segmentation network  $S$  having parameters  $\theta_S$  and whose goal is to recover the correct segmentation map  $\mathbf{y}$  given the encoded image  $\mathbf{z}$ . During

training, both  $\mathbf{z}_i$  and  $\mathbf{z}_j$  are segmented.

#### Training losses

Like most adversarial model, our system is trained with two losses that steers the model in opposite directions. In our case, the training procedure involves a segmentation loss and an adversarial loss :

$$\min_{\theta_E, \theta_S} \max_{\theta_D} \mathcal{L}(\theta_E, \theta_S, \theta_D) = \mathbb{E}_{\mathbf{x}, \mathbf{y} \sim \mathcal{X}, \mathcal{Y}} [\mathcal{L}_{\text{seg}}(S(E(\mathbf{x})), \mathbf{y})] - \lambda \mathbb{E}_{\mathbf{x}_i, \mathbf{x}_j \sim \mathcal{X}^2} [\mathcal{L}_{\text{adv}}(\mathbf{x}_i, \mathbf{x}_j, s_{ij}; \theta_D, \theta_E)] \quad (1)$$

where  $\mathcal{L}_{\text{seg}}$  is attached to the segmentation network,  $\mathcal{L}_{\text{adv}}$  is attached to the discriminator, and  $s_{ij} = \mathbb{1}(\text{id}(\mathbf{x}_i) = \text{id}(\mathbf{x}_j))$  is a binary indicator function indicating if two images come from the same person or not.

Using  $\hat{\mathbf{y}} = S(E(\mathbf{x}))$  as shorthand notation for the predicted segmentation map, we employ the generalized Dice loss (Sudre et al. 2017) to train the segmentation network, i.e.

$$\mathcal{L}_{\text{seg}}(\hat{\mathbf{y}}, \mathbf{y}) = 1 - \frac{2 \sum_p y_p \hat{y}_p}{\sum_p y_p + \sum_p \hat{y}_p}. \quad (2)$$

For the adversarial loss, we want the discriminator to differentiate subject identity in pairs of non-encoded images  $(\mathbf{x}_i, \mathbf{x}_j)$ , encoded images  $(\mathbf{z}_i, \mathbf{z}_j)$  or a mix of both  $(\mathbf{x}_i, \mathbf{z}_j)$ . Since the encoded images are outputted by  $E$ , we can formulate this loss as

$$\mathcal{L}_{\text{adv}}(\mathbf{x}_i, \mathbf{x}_j, s_{ij}; \theta_D, \theta_E) = \mathcal{L}_{\text{dis}}(D(\mathbf{x}_i, \mathbf{x}_j), s_{ij}) + \mathcal{L}_{\text{dis}}(D(E(\mathbf{x}_i), \mathbf{x}_j), s_{ij}) + \mathcal{L}_{\text{dis}}(D(E(\mathbf{x}_i), E(\mathbf{x}_j)), s_{ij}). \quad (3)$$

Here, the discriminator loss  $\mathcal{L}_{\text{dis}}$  is a binary cross entropy:

$$\mathcal{L}_{\text{dis}}(\hat{s}, s) = -s \log \hat{s} - (1 - s) \log(1 - \hat{s}). \quad (4)$$

Like most adversarial models, the parameters of our system cannot be updated all at once through a gradient step. Instead, we first update the encoder and segmentation parameters  $\theta_D, \theta_E$  by taking the following gradient descent step:

$$(\theta_S^{t+1}, \theta_E^{t+1}) \leftarrow (\theta_S^t, \theta_E^t) - \eta \nabla \tilde{\mathcal{L}}(\theta_S^t, \theta_E^t). \quad (5)$$

The gradient is estimated using random batches of image pairs  $\mathcal{B} \subset |\mathcal{X}| \times |\mathcal{X}|$ , as follows:

$$\nabla \tilde{\mathcal{L}}(\theta_E, \theta_S) = \frac{1}{|\mathcal{B}|} \sum_{(i,j) \in \mathcal{B}} \nabla_{\theta_E, \theta_S} [\mathcal{L}_{\text{seg}}(\hat{\mathbf{y}}_i, \mathbf{y}_i) - \lambda \mathcal{L}_{\text{dis}}(D(E(\mathbf{x}_i), \mathbf{x}_j), s_{ij}) - \lambda \mathcal{L}_{\text{dis}}(D(E(\mathbf{x}_i), E(\mathbf{x}_j)), s_{ij})] \quad (6)$$

We then update the discriminator parameters by taking a gradient ascent step

$$\theta_D^{t+1} \leftarrow \theta_D^t + \eta \nabla \tilde{\mathcal{L}}(\theta_D^t) \quad (7)$$

with the batch gradient computed as

$$\nabla \tilde{\mathcal{L}}(\theta_D) = -\frac{\lambda}{|\mathcal{B}|} \sum_{(i,j) \in \mathcal{B}} \nabla_{\theta_D} [\mathcal{L}_{\text{dis}}(D(\mathbf{x}_i, \mathbf{x}_j), s_{ij}) + \mathcal{L}_{\text{dis}}(D(E(\mathbf{x}_i), \mathbf{x}_j), s_{ij}) + \mathcal{L}_{\text{dis}}(D(E(\mathbf{x}_i), E(\mathbf{x}_j)), s_{ij})]. \quad (8)$$

Details of our training method are shown in Algo. 1.

---

**Algorithm 1:** Privacy-preserving network learning

---

**Input:** Images  $\mathcal{X}$  and ground-truth masks  $\mathcal{Y}$   
**Output:** Network parameters  $\theta_E, \theta_D, \theta_S$

```
/* Initialization */
Initialize network parameters  $\theta_E, \theta_D, \theta_S$ ;

/* Main loop */
for epoch = 1, \dots, E_{\max} do
  for iter = 1, \dots, T_{\max} do
    Randomly select batch  $\mathcal{B} \subset |\mathcal{X}| \times |\mathcal{X}|$ ;
    Update encoder and segmentation network
      parameters  $(\theta_S, \theta_E)$  using Eq. (5) and (6);
    Update discriminator parameters  $(\theta_D)$  using Eq.
      (7) and (8);
  return  $\theta_E, \theta_D, \theta_S$ ;
```

---

## Implementation Details

In this study, we used a U-Net architecture as in (Ronneberger, Fischer, and Brox 2015) but with 3D convolution kernels both for the encoder and the segmentation network. The discriminator is a Siamese network as in (Koch, Zemel, and Salakhutdinov 2015). We used a DenseNet architecture (Huang, Liu, and Weinberger 2017) with 3D convolution kernels for the CNN backbone. The CNN Siamese backbone (i.e. the left-most CNN inside the Discriminator box in Fig. 1) is used to extract the features of input images. The last layer of the discriminator contains two fully-connected layers to predict if two images are from the same patient. Further details on the networks are reported in the supplementary material.

The system was implemented with Pytorch. We used the Adam optimizer with a learning rate of  $10^{-4}$  for the whole training process. The PC used for training is an Intel(R) Core(TM) i7-6700K 4.0GHz CPU, equipped with a NVIDIA GeForce GTX 1080Ti GPU with 12 GB of memory. The training our networks takes roughly 30 minutes per epoch, and around 2 days for the fully-trained system.

Since our networks employ 3D convolutions, and due to the large size of MRI volumes, dense training cannot be applied to the whole volume. Instead, volumes are split into smaller patches of  $64 \times 64 \times 64$ , which allows dense training in our hardware setting. The encoder is initialized with the weights of an auto-encoder, the segmentation network was pre-trained on the original images and the discriminator was pre-trained on the PPMI dataset.

## 4 Experimental results

### Datasets

**PPMI** We experiment on brain tissue segmentation of 5 classes: white matter (WM), gray matter (GM), nuclei, internal cerebrospinal fluid (CSF int.) and external cerebrospinal fluid (CSF ext.). We used the T1 images of the publicly-available Parkinson’s Progression Marker Initiative (PPMI) dataset (Marek et al. 2011). We took images from 350 subjects, most of which with a recently diagnosed Parkinson

	Training	Testing	Total
Nb subjects	269	81	350
Nb images	592	181	773
Nb positive pairs	509	148	657

Table 1: PPMI data used for training and testing our method.

disease. Each subject underwent one or two baseline acquisitions and one or two acquisitions 12 months later for a total of 773 images. PPMI MR images were acquired with standardized protocol used on Siemens Tim Trio and Siemens Verio 3 Tesla machines from 32 different sites. The images have been registered onto a common MNI space and resized to  $144 \times 192 \times 160$  with a  $1 \text{ mm}^3$  resolution. More information on the MRI acquisition and processing can be found online: [www.ppmi-info.org](http://www.ppmi-info.org).

The dataset was divided into a training and a testing part as shown in Table 1. In order to keep a good balance between the pair of images, during training and testing, we randomly sampled and equal number of negative and positive samples. The segmentation ground-truth has been obtained with Freesurfer.

**MRBrainS** To further validate the proposed method and investigate its generalization ability, we also tested it on segmenting MRI scans from the MRBrainS 2013 challenge dataset (Mendrik et al. 2015). These images were acquired on a 3.0T Philips Achieva MR scanner and come with expert-annotated segmentation masks including three classes: WM, GM and CSF. We employed a single modality (i.e., MR-T1) in our experiments. Bias correction was performed as a pre-processing step. Original images had a resolution of  $0.96 \times 0.96 \times 3 \text{ mm}^3$  and were registered onto the MNI space using ANTs (Avants et al. 2011).

### Evaluation metrics

To gauge the performance of our system, we use the classification accuracy for the discriminator and the Dice score for the segmentation results. We also use the MS-SSIM score to measure image-to-image distance as a proxy of perceived image quality (Wang, Simoncelli, and Bovik 2003).

### Results

**Baseline results** At first, we processed the dataset without the adversarial component, i.e. by independently training the segmentation and the discriminator networks without the encoder. We call this setting *Baseline* in our results. In the first row of Table 2, we see that the discriminator obtains a testing accuracy of 95.3%. This underlines how easy it is for a neural network to recognize a patient based on the content of a brain MRI. More surprising is the 97% classification accuracy that we get by simply thresholding the image-to-image MS-SSIM score. This can be explained by the inter- and intra-subject MS-SSIM distribution plots shown in the third row of the first column of Fig. 2. As can be seen, when considering non-encoded images, the intra-subject MS-SSIM scores (red curve) are significantly larger than that of the inter-subjects (blue curve). This again illus-

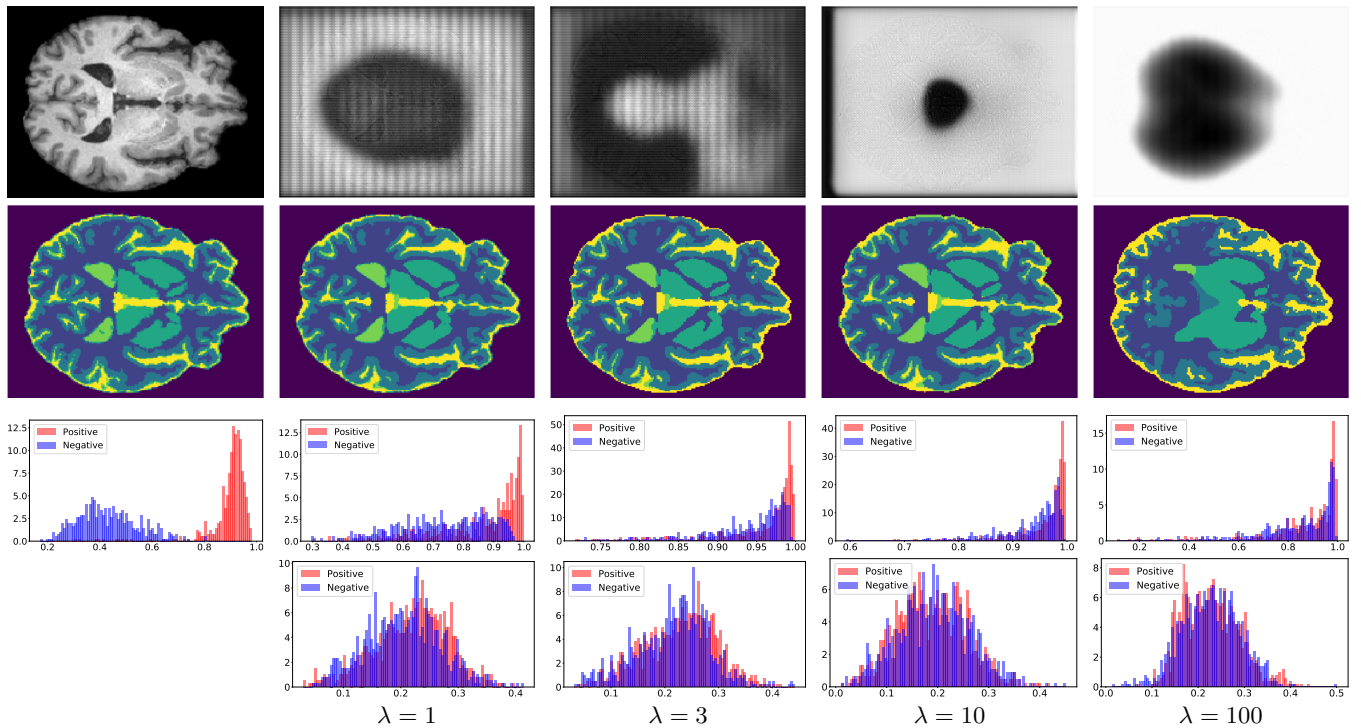


Figure 2: Impact of discriminator loss ( $\lambda$ ). **[First column]** (Top row): input MRI image  $\mathbf{x}$ , (Second row): ground truth segmentation map  $\mathbf{y}$ , (Third row): distribution of inter- and intra-subject MS-SSIM score on the PPMI dataset. **[Remaining columns]**, (Top row): encoded image  $\mathbf{z}$ , (Second row): predicted segmentation  $\hat{\mathbf{y}}$  and (Third row): distribution of MS-SSIM values between encoded images ( $z_i, z_j$ ) (Last row): distribution of MS-SSIM values between non-encoded and encoded images ( $x_i, z_j$ ).

trate the ease of recognizing the identity of a person based on the content of a medical image.

The PPMI segmentation baseline Dice scores for the five regions are in the first row of Table 3. We also report the overall Dice computed as the mean of Dice scores in all regions, weighted by the regions’ size. These results correspond roughly to those obtained in recent publications (Dolz et al. 2019). Note that the nuclei and the internal CSF have a lower Dice due to the smaller size of these regions.

		Discr.	MS-SSIM
$(\mathbf{x}_i, \mathbf{x}_j)$	—	0.953	0.970
	$\lambda=1$	0.520	0.564
$(\mathbf{z}_i, \mathbf{z}_j)$	$\lambda=1$	0.520	0.564
	$\lambda=3$	0.537	0.533
	$\lambda=10$	0.523	0.510
	$\lambda=100$	0.516	0.503
$(\mathbf{x}_i, \mathbf{z}_j)$	$\lambda=1$	0.557	0.686
	$\lambda=3$	0.517	0.662
	$\lambda=10$	0.531	0.611
	$\lambda=100$	0.524	0.527

Table 2: Same-subject prediction accuracy on test examples using the discriminator or by thresholding MS-SSIM scores. Performance is reported for pairs of non-encoded images ( $\mathbf{x}_i, \mathbf{x}_j$ ), pairs of encoded images ( $\mathbf{z}_i, \mathbf{z}_j$ ) or mixed pairs ( $\mathbf{x}_i, \mathbf{z}_j$ ), and for different  $\lambda$  values.

	GM	WM	Nuclei	CSF int.	CSF ext.	Overall
Baseline	0.941	0.853	0.657	0.665	0.825	0.848
$\lambda=1$	0.925	0.824	0.580	0.598	0.752	0.812
$\lambda=3$	0.899	0.793	0.549	0.550	0.693	0.778
$\lambda=10$	0.881	0.796	0.555	0.531	0.685	0.771
$\lambda=100$	0.847	0.692	0.454	0.405	0.513	0.684

Table 3: Segmentation Dice score on the PPMI test set for different values of  $\lambda$ . Baseline refers to the model trained with non-encoded images.

**Adversarial results** We report adversarial results obtained with different values of parameter  $\lambda$ , which controls the trade-off between segmentation accuracy and identity obfuscation. The first row of Fig. 2 shows encoded images  $\mathbf{z}$  next to the raw input MRI  $\mathbf{x}$ . As can be seen, the larger the  $\lambda$  value is, the more distorted the encoded image gets. Nonetheless, except for extreme cases (e.g.,  $\lambda = 100$ ) the encoded images contain enough information for the segmentation network to recover a good segmentation map (c.f., the second row of Fig. 2). The obfuscating power of our method is also illustrated by the MS-SSIM plots (c.f., the last two rows of Fig. 2). As  $\lambda$  increases, the distribution of inter-subject MS-SSIM between encoded images ( $z_i, z_j$ ) becomes more and more similar to that of intra-subjects. The same situation appears between non-encoded and encoded images ( $x_i, z_j$ ). The recognition scores in Table 2 show the same trend, with

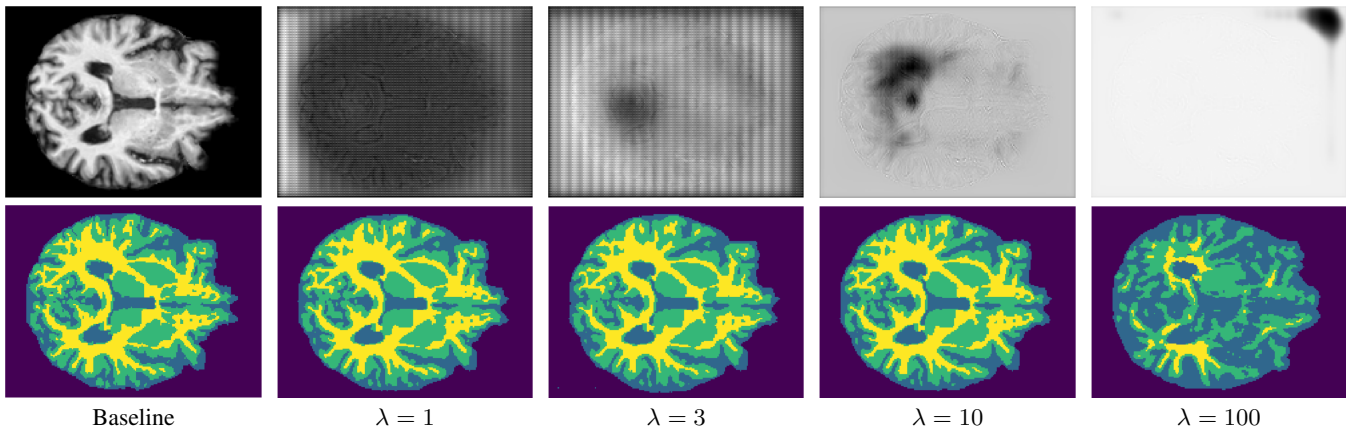


Figure 3: Test results on the MRBrainS dataset. **[First column]** (Top row): input MRI image  $\mathbf{x}$ , (Bottom row): ground truth segmentation map  $\mathbf{y}$ . **[Remaining columns]**, (Top row): encoded image  $\mathbf{z}$ , (Bottom row): predicted segmentation  $\hat{\mathbf{y}}$  with re-trained segmentation networks on MRBrainS

MS-SSIM classification rates dropping as  $\lambda$  increases.

These results underline the fact that the encoder does not only change image intensity values, but also the structure of the image. Our system thus prevents from recognizing the identity of a patient both when considering an encoded image pair  $(\mathbf{z}_i, \mathbf{z}_j)$  as well as an encoded and non-encoded image pair  $(\mathbf{x}_i, \mathbf{z}_j)$ . Furthermore, despite these structural changes, the segmentation network can still recover good segmentation maps, even for  $\lambda=10$  (c.f., Table 3).

**Generalization to newly acquired data** A large dataset such as PPMI with per-patient longitudinal data is required to train end-to-end our system. However, once trained, the encoder can be fixed and used as an identity obfuscation module to train the segmentation network on newly acquired images. In order to illustrate this, we used images from the MRBrainS dataset which were acquired with a different acquisition protocol than PPMI and have three labels instead of five, i.e., WM, GM, and CSF.

We first tested on MRBrainS images our model pre-trained with PPMI data. In order to match the three-class ground-truth, we merged the CSF int. and CSF ext. outputs into a single CSF class, and the GM and nuclei outputs into a single GM class. Results for different  $\lambda$  values are shown at the top of Table 4. As expected, these results are slightly worse than those on PPMI (see Table 3).

However, as can be seen at the bottom of Table 4, segmentation accuracy improves when retraining the segmentation network on MRBrainS data while keeping the encoder fixed. This shows that the segmentation network of our system can be updated, even after being deployed onto a cloud server. Segmentation maps as well as encoded MRBrainS images are given in Fig 3.

**Robustness analysis** To make sure that our system does not work only on high-quality images such as those of PPMI, we performed a robustness analysis where we trained our method on the original PPMI dataset (with  $\lambda=1$ ) and tested it on noisy versions of the PPMI test images or on images with a lower  $2 \times 2 \times 2 \text{ cm}^3$  resolution. Results are provided

		GM	WM	CSF	Overall
No retrain	$\lambda=1$	0.768	0.822	0.804	0.796
	$\lambda=3$	0.767	0.852	0.798	0.804
	$\lambda=10$	0.757	0.798	0.768	0.772
	$\lambda=100$	0.499	0.464	0.648	0.537
Retrain	$\lambda=1$	0.819	0.827	0.823	0.821
	$\lambda=3$	0.794	0.807	0.831	0.814
	$\lambda=10$	0.780	0.747	0.797	0.790
	$\lambda=100$	0.605	0.360	0.572	0.586

Table 4: Segmentation Dice score on the MRBrainS dataset for different values of  $\lambda$ . (Top) The networks has not been retrained on MRBrainS images (Bottom) only the segmentation network has been retrained, the encoded.

	GM	WM	Nuclei	CSF int.	CSF ext.	Overall
Noise (15dB)	0.921	0.818	0.572	0.585	0.743	0.808
Noise (10dB)	0.917	0.804	0.566	0.582	0.696	0.797
Noise (5dB)	0.821	0.706	0.514	0.472	0.331	0.669
Low res.	0.881	0.781	0.552	0.516	0.683	0.759

Table 5: Segmentation Dice score on PPMI dataset with different levels of Rician noise (measured in SNR dB) and low resolution setting.

in Fig. 4 and Table 5. As can be seen, the encoding and segmentation is not much affected by noise. The segmentation accuracy is close to the one obtained on the original PPMI test set, with overall Dice scores around 80% for noisy images with an SNR of 15db or 10db. Reducing image resolution seems to induce more significant changes in the encoding, however the segmentation network appears robust to these changes.

**Runtime** In terms of runtime, an average of 0.08 second is required to encode an image on a NVIDIA GTX 1080Ti, whereas the entire segmentation process requires around 0.1 seconds per image. This runtime is negligible compared to the 8 to 12 hours required by Freesurfer. Training curves

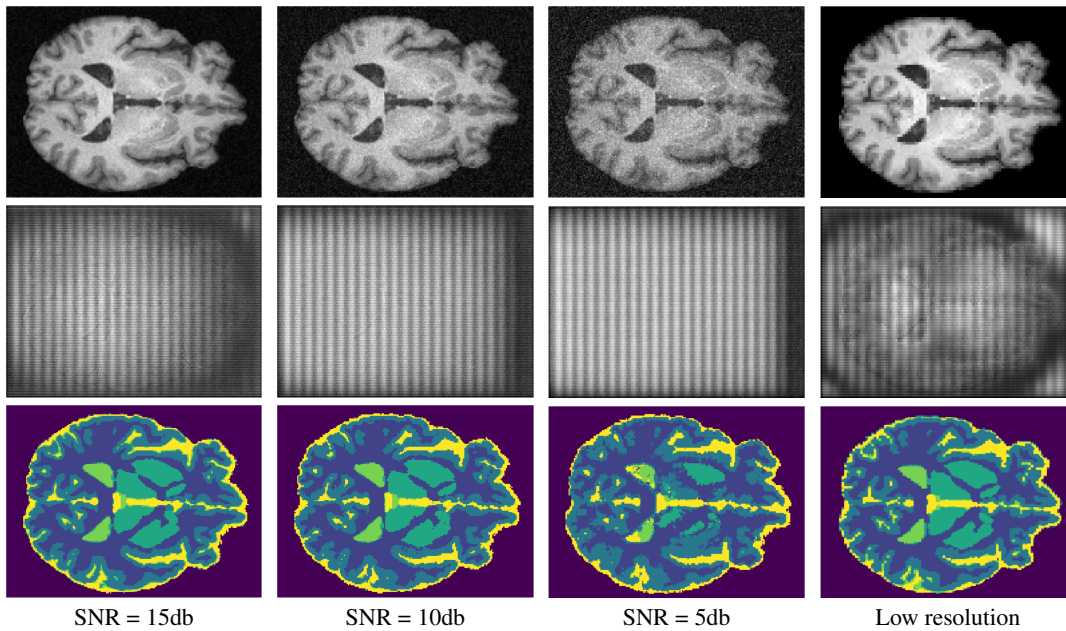


Figure 4: Segmentation with different noise level and a lower resolution setting. (Top row): Degraded images, (Middle row): Encoded images, (Bottom row): Segmentation Results

illustrating the evolution of different loss terms and performance metrics can be found in the supplementary material.

## 5 Discussion and conclusion

In this work, we presented a novel framework which integrates an encoder, a segmentation CNN and a Siamese network to preserve the privacy of medical imaging data. Experimental results on two independent datasets have shown that the proposed method can preserve the identity of a patient while maintaining the performance on the target task. While this is an interesting application *per se*, it opens the door to appealing potential uses. For example, this approach can be integrated in a continual learning scenario trained on a decentralized dataset, where images have to be shared across institutions but privacy needs to be preserved. From a clinical perspective, obfuscating visual data in addition to current anonymization techniques may foster multi-centre collaborations, resulting in larger datasets as well as more complete and heterogeneous clinical studies.

Additionally, we have shown that the proposed privacy-preserving model generalizes well to novel datasets, unlike similar works (Chen, Konrad, and Ishwar 2018) which cannot generalize to encoded images of subjects not seen in training. This facilitates the scalability of our approach to new datasets or tasks. As preliminary step towards preventing privacy leakage in medical imaging data, this study has however some limitations. For example, the domain shift between employed datasets is not significantly large, since both include MRI images of adult brains (even though the acquisition protocols and parameters across scanners differ). Although similar domain shift has resulted in a performance degradation in segmentation networks (Dolz, Desrosiers, and Ayed 2018), results demonstrate the good generability of the proposed method in these cases. Future investigations

will explore the generalization capabilities of the trained encoder on datasets where the domain shift is larger, for example, between infant and adult brains or even between different image modalities such as MRI and CT.

## Acknowledgements

We acknowledge the support of the Natural Sciences and Engineering Research Council of Canada (NSERC), and thank NVIDIA corporation for supporting this work through their GPU grant program.

## References

- [Avants et al. 2011] Avants, B.; Tustison, N.; Song, G.; Cook, P.; Klein, A.; and Gee, J. 2011. A reproducible evaluation of ants similarity metric performance in brain image registration. *Neuroimage* 54(3):2033–2044.
- [Butler et al. 2015] Butler, D. J.; Huang, J.; Roesner, F.; and Cakmak, M. 2015. The privacy-utility tradeoff for remotely teleoperated robots. In *Proc of ACM/IEEE ICHRI*, 27–34.
- [Chen et al. 2016] Chen, J.; Wu, J.; Richter, K.; Konrad, J.; and Ishwar, P. 2016. Estimating head pose orientation using extremely low resolution images. In *proc of IEEE SSIAT*, 65–68.
- [Chen, Konrad, and Ishwar 2018] Chen, J.; Konrad, J.; and Ishwar, P. 2018. Vgan-based image representation learning for privacy-preserving facial expression recognition. In *Proc of CVPR-W*, 1570–1579.
- [Dai et al. 2015] Dai, J.; Saghafi, B.; Wu, J.; Konrad, J.; and Ishwar, P. 2015. Towards privacy-preserving recognition of human activities. In *proc of ICIP*, 4238–4242.
- [Dolz et al. 2019] Dolz, J.; Gopinath, K.; Yuan, J.; Lombaert, H.; Desrosiers, C.; and Ben Ayed, I. 2019. Hyperdense-

- net: A hyper-densely connected CNN for multi-modal image segmentation. *IEEE TMI* 38(5):1116–1126.
- [Dolz, Desrosiers, and Ayed 2018] Dolz, J.; Desrosiers, C.; and Ayed, I. B. 2018. 3D fully convolutional networks for subcortical segmentation in MRI: A large-scale study. *NeuroImage* 170:456–470.
- [Ganin et al. 2016] Ganin, Y.; Ustinova, E.; Ajakan, H.; Germain, P.; Larochelle, H.; Laviolette, F.; Marchand, M.; and Lempitsky, V. 2016. Domain-adversarial training of neural networks. *JMLR* 17(1):2096–2030.
- [Goodfellow et al. 2014] Goodfellow, I.; Pouget-Abadie, J.; Mirza, M.; Xu, B.; Warde-Farley, D.; Ozair, S.; Courville, A.; and Bengio, Y. 2014. Generative adversarial nets. In *proc NIPS*, 2672–2680.
- [Hesamifard, Takabi, and Ghasemi 2017] Hesamifard, E.; Takabi, H.; and Ghasemi, M. 2017. Cryptodl: Deep neural networks over encrypted data. *CoRR* abs/1711.05189.
- [Hsu, Lu, and Pei 2011] Hsu, C.-Y.; Lu, C.-S.; and Pei, S.-C. 2011. Homomorphic encryption-based secure SIFT for privacy-preserving feature extraction. In *proc of MWSF-III*, volume 7880.
- [Huang, Liu, and Weinberger 2017] Huang, G.; Liu, Z.; and Weinberger, K. Q. 2017. Densely connected convolutional networks. In *proc CVPR*.
- [Jalal, Uddin, and Kim 2012] Jalal, A.; Uddin, M. Z.; and Kim, T.-S. 2012. Depth video-based human activity recognition system using translation and scaling invariant features for life logging at smart home. *IEEE TCE* 58(3):863–871.
- [Koch, Zemel, and Salakhutdinov 2015] Koch, G.; Zemel, R.; and Salakhutdinov, R. 2015. Siamese neural networks for one-shot image recognition. In *proc of ICML*.
- [Konečný et al. 2016] Konečný, J.; McMahan, H. B.; Ramage, D.; and Richtárik, P. 2016. Federated optimization: Distributed machine learning for on-device intelligence. *CoRR* abs/1610.02527.
- [Kumar et al. 2018] Kumar, K.; Toews, M.; Chauvin, L.; Colliot, O.; and Desrosiers, C. 2018. Multi-modal brain fingerprinting: A manifold approximation based framework. *NeuroImage* 183:212 – 226.
- [Litjens et al. 2017] Litjens, G.; Kooi, T.; Bejnordi, B. E.; Setio, A. A. A.; Ciompi, F.; Ghafoorian, M.; Van Der Laak, J. A.; Van Ginneken, B.; and Sánchez, C. I. 2017. A survey on deep learning in medical image analysis. *MedIA* 42:60–88.
- [Luc et al. 2016] Luc, P.; Couprie, C.; Chintala, S.; and Verbeek, J. 2016. Semantic segmentation using adversarial networks. *CoRR* abs/1611.08408.
- [Marek et al. 2011] Marek, K.; Jennings, D.; Lasch, S.; Siderowf, A.; Tanner, C.; Simuni, T.; Coffey, C.; Kiebertz, K.; Flagg, E.; Chowdhury, S.; et al. 2011. The parkinson progression marker initiative (ppmi). *Progress in neurobiology* 95(4):629–635.
- [McClure et al. 2018] McClure, P.; Zheng, C. Y.; Kaczmarzyk, J.; Rogers-Lee, J.; Ghosh, S.; Nielson, D.; Bandettini, P. A.; and Pereira, F. 2018. Distributed weight consolidation: A brain segmentation case study. In *proc of NIPS*, 4093–4103.
- [McMahan et al. 2016] McMahan, H. B.; Moore, E.; Ramage, D.; and Arcas, B. A. 2016. Federated learning of deep networks using model averaging. *CoRR* abs/1602.05629.
- [McMahan et al. 2017] McMahan, H.; Moore, E.; Ramage, D.; Hampson, S.; and B.A. 2017. Fast trust region for segmentation. In *Proc of ICAIS*, 1273–1282.
- [Mendrik et al. 2015] Mendrik, A. M.; Vincken, K. L.; Kuijff, H. J.; Breeuwer, M.; Bouvy, W. H.; De Bresser, J.; Alansary, A.; De Bruijne, M.; Carass, A.; El-Baz, A.; et al. 2015. MR-BrainS challenge: online evaluation framework for brain image segmentation in 3T MRI scans. *Comp. Intel. and Neuro.* 2015:1.
- [Oleszkiewicz et al. 2018] Oleszkiewicz, W.; Kairouz, P.; Piczak, K.; Rajagopal, R.; and Trzciński, T. 2018. Siamese generative adversarial privatizer for biometric data. In *proc of ACCV*, 482–497.
- [Paillier 1999] Paillier, P. 1999. Public-key cryptosystems based on composite degree residuosity classes. In *proc IC-TACT*, 223–238.
- [Pittaluga, Koppal, and Chakrabarti 2019] Pittaluga, F.; Koppal, S.; and Chakrabarti, A. 2019. Learning privacy preserving encodings through adversarial training. In *proc of IEEE WACV*, 791–799.
- [Raval, Machanavajjhala, and Cox 2017] Raval, N.; Machanavajjhala, A.; and Cox, L. P. 2017. Protecting visual secrets using adversarial nets. In *proc of CVPRW*, 1329–1332.
- [Ronneberger, Fischer, and Brox 2015] Ronneberger, O.; Fischer, P.; and Brox, T. 2015. U-net: Convolutional networks for biomedical image segmentation. *CoRR* abs/1505.04597.
- [Roy and Boddeti 2019] Roy, P. C., and Boddeti, V. N. 2019. Mitigating information leakage in image representations: A maximum entropy approach. *CoRR* abs/1904.05514.
- [Sudre et al. 2017] Sudre, C. H.; Li, W.; Vercauteren, T.; Ourselin, S.; and Cardoso, M. J. 2017. Generalised dice overlap as a deep learning loss function for highly unbalanced segmentations. *CoRR* abs/1707.03237.
- [Vepakomma et al. 2018] Vepakomma, P.; Swedish, T.; Raskar, R.; Gupta, O.; and Dubey, A. 2018. No peek: A survey of private distributed deep learning. *CoRR* abs/1812.03288.
- [Wang et al. 2017] Wang, W.; Vong, C.-M.; Yang, Y.; and Wong, P.-K. 2017. Encrypted image classification based on multilayer extreme learning machine. *MSSP* 28(3):851–865.
- [Wang, Simoncelli, and Bovik 2003] Wang, Z.; Simoncelli, E. P.; and Bovik, A. C. 2003. Multiscale structural similarity for image quality assessment. In *proc of IEEE ACSSC*, 1398–1402.
- [Wu et al. 2018] Wu, Z.; Wang, Z.; Wang, Z.; and Jin, H. 2018. Towards privacy-preserving visual recognition via adversarial training: A pilot study. In *proc of ECCV*, 606–624.



- [Xie et al. 2014] Xie, P.; Bilenko, M.; Finley, T.; Gilad-Bachrach, R.; Lauter, K. E.; and Naehrig, M. 2014. Crypto-nets: Neural networks over encrypted data. *CoRR* abs/1412.6181.
- [Xu et al. 2019] Xu, C.; Ren, J.; Zhang, D.; Zhang, Y.; Qin, Z.; and Ren, K. 2019. GANobfuscator: Mitigating information leakage under gan via differential privacy. *IEEE TIFS* 14(9):2358–2371.
- [Yang et al. 2018] Yang, T.-Y.; Brinton, C.; Mittal, P.; Chiang, M.; and Lan, A. 2018. Learning informative and private representations via generative adversarial networks. In *proc of ICBD*, 1534–1543.
- [Yang et al. 2019] Yang, Q.; Liu, Y.; Chen, T.; and Tong, Y. 2019. Federated machine learning: Concept and applications. *ACM Transactions on Intelligent Systems and Technology (TIST)* 10(2):12.
- [Zhou, Greenspan, and Shen 2017] Zhou, S.; Greenspan, H.; and Shen, D. 2017. *Deep Learning for Medical Image Analysis*. Elsevier Science.
- [Ziad et al. 2016] Ziad, M. T. I.; Alanwar, A.; Alzantot, M.; and Srivastava, M. 2016. Cryptoimg: Privacy preserving processing over encrypted images. In *proc of IEEE CNS*, 570–575.